ELSEVIER

Contents lists available at ScienceDirect

Tunnelling and Underground Space Technology incorporating Trenchless Technology Research

journal homepage: www.elsevier.com/locate/tust



Distributed temperature sensor model for linear heat detection in tunnel fires

Jakub Bielawski ^{a,b}, Dia Luan ^{b,c}, Xiaoning Zhang ^b, Weikang Xie ^b, Xinyan Huang ^b, Wojciech Węgrzyński ^{a,*}

- ^a Building Research Institute, Fire Research Department, Warsaw, Poland
- b Department of Building Environment and Energy Engineering, The Hong Kong Polytechnic University, Hong Kong, China
- ^c Department of Fire Protection Engineering, Southwest Jiaotong University, Chengdu, Sichuan, China

ARTICLE INFO

Keywords: DTS Linear heat detection Tunnel fire Fire detection CFD fire model Fiber optical sensor

ABSTRACT

This study proposes a method for implementing distributed temperature sensing systems in tunnel fire simulations. A review of the investigations was conducted, and previous research on linear heat detection was examined. The characteristics and operational parameters of a complete DTS-based LHD system in a road tunnel are presented. A heat transfer model of the DTS sensor cable for CFD modelling was developed based on experiments in the standardised EN 54–5 wind tunnel for testing heat sensors. Based on the data analysis, substitute physical properties of the sensor cable were selected for the heat transfer model to allow implementation of the DTS model in CFD. Concurrently, an RTI value of 90 $(m/s)^{1/2}$ was approximated to compare the model with the response-time model commonly used in fire engineering analyses. To validate the model, two full-scale fire tests were carried out in a road tunnel in Świnoujście, Poland, and CFD numerical simulations were performed with the proposed DTS model. The relative error of detection time prediction was within 3% for the case with low velocity, and successfully predicted no detection in the case with high velocity (>1 m/s). The developed model allows to tracking temperature changes of the DTS sensor cable with satisfactory precision and can be applied in various tunnel fire analyses.

1. Introduction

1.1. Rationale and scope

Reliable and fast fire detection in tunnels is the key to properly activating other fire and life safety systems, including smoke control, fixed firefighting and suppression systems, evacuation lighting, and alarm and voice alarm systems. Due to challenging environmental conditions inside the tunnel, standard smoke detection systems (point and linear smoke detectors) may not be used. Consequently, multiple fire detection technologies have been developed and applied in tunnels, such as linear heat detection (LHD), flame detection, visual image processing, point heat sensors, and CO_2/CO sensors. Each type has a different specification and detection mechanism (Ingason et al., 2015). In European countries, linear heat detection is the prevalent technology that provides sufficient spatial and temporal resolution for measurement. Following the EN 54–22 standard (EN 54-22:, 2020), LHD is

classified either as an integrating or non-integrating system. In the first case, the temperature response is summed up in a certain way over the length of the sensing element. An example of an integrating system is an aspirating system that probes the tunnel's air. The output signal depends on the local temperature effect in the non-integrating type. This makes it possible to track local temperature distribution changes, including systems based on fiber optics. The most common types of LHD systems are methods based on a fiber Bragg grating (FBG) or a Raman scattering distributed temperature sensing (DTS). These systems differ in local resolution, maximum sensor element length, and typical measuring point distance. This study presents an investigation of LHD based on Raman scattering DTS, and a physical explanation of the system is presented in Section 2.

The DTS system is located underneath the tunnel ceiling. It measures the air temperature in the surroundings of the cable, assuming that the hot smoke layer and ceiling jets caused by fire will be most pronounced in this region (Li et al., 2011; He, 2021; Luan, 2021; Zeng et al., 2023).

E-mail addresses: j.bielawski@itb.pl (J. Bielawski), luandie@swjtu.edu.cn (D. Luan), xiaon.zhang@connect.polyu.hk (X. Zhang), weikang.xie@polyu.edu.hk (W. Xie), xy.huang@polyu.edu.hk (X. Huang), w.wegrzynski@itb.pl (W. Węgrzyński).

 $^{^{\}star}$ Corresponding author.

The temperature indicated by the sensor is affected by the heat transfer processes – primarily the convective and radiative heat transfer from the gas to the cable, conductive heat losses from the cable, and the heat transfer process from the sheathing to the interior of the cable. Depending on the construction of the cable and its thermal bulk, different cables may show different responses to the gas temperature. The fire alarm is triggered when either the measured temperature exceeds the temperature threshold, or the critical growth rate of the temperature exceeds the limiting value. Additional conditions, such as time-averaging or coincidence logic, are commonly applied to protect against false alarms.

Due to the aggressive tunnel environment, the DTS is protected by additional sheeting layers. This influences the heat transfer processes and, in effect, the measured temperature, potentially causing lag in detecting the fire. The lag may also be more pronounced due to the strong flows inside the tunnel caused by the piston effect of the road traffic (Król et al., 2023; Liang et al., 2021; Bari and Naser, 2010), natural draught (Król et al., 2019), flows driven by the chimney effect, or the wind (Luan, 2021; Wegrzyński and Lipecki, 2018; Ingason et al., 2012; Chen, 2020). Airflow structure could vary depending on ventilation system characteristics (Król et al., 2024). In the presence of the longitudinal flow, the smoke temperature will be reduced due to the entrainment of cold air into the smoke plume. At the same time, the convective heat transfer to the cable may be increased (compared to quiescent conditions at the same temperature). Another effect of the longitudinal flow is the potential to carry smoke downstream, causing the fire to be detected further away from the physical location of the source of the fire.

Studying complex interactions between the fire, flow, and the DTS sensor response at full scale is prohibitively expensive, and the experiments are usually limited to a few runs (Ingason, 2015; Liu et al., 2011). This is especially problematic if one wants to determine the sensor performance for an extensive range of flow velocities, fire growth rates, and peak Heat Release Rates (HRR) (Zhang, 2021). CFD modelling is a potential tool to allow for complex sensitivity studies on the impact of the abovementioned variables. Furthermore, the CFD is routinely used to assess longitudinal ventilation performance in contemporary tunnel engineering. If the DTS model is added to such simulation, it may enable more realistic fire scenarios and could allow for the implementation of sensor logic in the studies.

In the current study we propose a numerical model of a LHD DTS sensor, based on a heat transfer solution for a thin object exposed to cross flow. Investigated DTS sensor is a representation of a dedicated application to real tunnels and is commonly used in Europe. To enable that, we have developed a numerical model of a fiber-optics distributed temperature sensing (DTS) technology and carried out laboratory experiments to determine the unknown thermophysical characteristics of the cable, as well as approximate its response time index (RTI) characteristic. The model was validated based on smoke detection tunnel measurements in small scale, and later in full scale in experiments carried out in a road tunnel. This model is not limited to a particular CFD code and can be used in a variety of calculation methods for fire plume parameters. Implementation of the model is described, as well as a simplified approach using the well-established RTI model, for which we found a satisfactory match at RTI value of 90 (m/s)^{1/2}. Finally, the proposed DTS model is employed in a full-scale CFD model of a road tunnel in Świnoujście and compared with the results of an experiment carried out by the Authors in this tunnel.

1.2. State-of-the-art

Linear Heat Detectors are defined by European standard EN 54–22, which covers requirements and testing protocols for resettable and line-type heat detectors. As a life safety system, LHD in the tunnel should pass fire detection performance formulated in international standards and guidelines such as NFPA (NFPA 72, 2022; NFPA 502, 2023), PIARC

(PIARC, 2007), RABT (RABT, 2006), RVS (RVS, 2019), NCHRP (NCHRP, 2017) or ASTRA (2007). These standards set precise requirements for the test fire HRR, maximum detection time, and distance from the fire origin for evaluating the LHD system at the commissioning of tunnels. To date, many researchers have investigated various factors affecting fire detection by LHDs in tunnels for performance-based design.

Liu et al. (2011a,b) performed a series of fire tests at the Laboratory tunnel and Carré-Viger tunnel in Montreal to compare functionality between selected types of fire detection systems for tunnel application. Fire scenarios considered following mock-up configurations: (a) small-unobstructed pool fires; (b) pool fires underneath a simulated vehicle; (c) pool fires behind a large vehicle; (d) engine compartment fires; (e) passenger compartment fires and (f) moving vehicle fires. In full-scale tests, the additional variable was longitudinal airflow. Results of the tests on the lab scale showed that LHD triggered alarms primarily based on the rate of temperature rise, and detection times were determined by fire size and fuel type. In the experiments with various airflow velocities, it was noticed that general detection times were delayed. The exception was the test with a large shielded fire, and obstruction caused the fire to increase under airflow conditions. Due to forced airflow, the hot spot at the ceiling was shifted downstream, up to 10 m from fire locations.

Ingason (2015) conducted a series of fire experiments in a laboratory tunnel and full-scale Swedish road tunnels to evaluate the performance of fire detection systems in the face of developing a simple, repeatable, and realistic evaluation method for the *Stockholm bypass* project. Fires with HRR in the range of 0.5-3.6 MW at longitudinal ventilation velocities of 1.5-7.7 m/s were performed in the Törnskog and Northern Link tunnels. As an outcome, a method using a petrol pool fire in a pan with a diameter of 0.6 m was proposed, which is suitable for wind speeds in the range of 2-6 m/s. The method is suitable for examining flame or smoke detectors, LHDs, and visual fire detection systems in tunnels.

Huijben (2002) conducted fire tests of the fiber optics and two other sensing cables containing electronic sensors at various fire HRR and size and airflow velocities. The maximum measured temperature values by the systems were in the range of 20–30 °C, while their location differed more than 20 m in the tests with airflow velocities in the range of 3–5 m/s. Compared to the results, it was concluded that slow-developing fires at airflow velocity below 1 m/s could be detected in 1–3 min if they are located directly beneath the sensing cable. If air velocity is more than 3 m/s, no detected alarms should be expected, or detection time will be more than 5 min. Fast-developing fires will nearly always be detected in 3 min, independent of the velocity.

Ciming et al. (2007) conducted fire tests on 13 connected FBG sensors with various Bragg wavelengths mounted transversely every 5.0 m at a height of 6.6 m above road level. The alarm thresholds set were fixed temperature vale 45 °C and rate-of-rise 0.2 °C/s. The sensor located directly above the fire was triggered in 10 s, and the adjacent sensors in up to 60 s. There was no information about longitudinal velocity during tests. It could be assumed that tests were conducted in approximately windless conditions, because utility tunnels have more stable airflow conditions.

A series of full-scale fire detection tests were carried out in the Runehamar tunnel, investigating the detection capabilities of the FBG sensors. 30 tests were carried out with gas burners and liquid pool fires (Li and Du, 2020). Results were compared with thermocouple measurements, and compared with a prediction model, highlighting the delay in temperature response of the BFG sensor. The tests shown that the sensor can be approximated to a bulb with RTI value of 57 (m/s) $^{1/2}$. The FBG cable measurement were also carried in CFD simulations (Li et al., 2020). Study shown differences between 9 % to 25 % between different sensor locations (central and side cables) for fires up to 1 MW. The modelling was carried with use of electrical cable failure model — THIEF (Thermally-Induced Electrical Failure) adopted in Fire Dynamics Simulator (FDS) software.

Lönnermark et al. (Lönnermark et al., 2008) investigated FBG capabilities for the measurement of gas temperature in scale-model tunnel

fires. FBG sensor was compared with thermocouples with varying diameters. The results show that the temperature measured by the FBG sensor is more accurate than the actual gas temperature of any of the examined thermocouples.

Researchers have also noticed the use of linear heat detection in utility tunnels, which are characterized by more stable airflow conditions. Ishii et al. (Ishii et al., 1997) examined fiber optics detection and proposed that the fire heat release rate could be estimated from the measured temperature distribution and conversion coefficient of the tunnel. Fan et al. (Fan et al., 2014) performed an experimental study with three types of LHD: differential/fixed sensing cable, distributed Raman fiber thermal detector (DTS), and fiber Bragg grating (FBG) thermal detector. The time to detection was about 30 s, and the recorded temperature rising rate was more than 5 °C/min. Guo et al. (Guo et al., 2024) performed a comparative study between different fire detectors in utility tunnels. LHD was found to have the best comprehensive detection effect due to the local nature of point fire detectors.

Following research done so far, we have observed a gap in the definition of the sensor properties for the purpose of CFD modelling. The literature studies focused on the sensor response for real-life scenarios rather than defining the measuring properties of the LHD sensors. The time delay of the sensor is not well-defined in the literature, especially with regard to the spatial arrangement of the fires against the sensors. While literature studies considering steady-state flow and small fire sources exist, we have not found a reliable source of knowledge regarding LHD detection in varying flow conditions. Using the DTS model presented in this study, could be conducted accurate analyses for various airflow scenarios like traffic coming to a stop and the piston effect decreasing in time (Król et al., 2023). Based on the research gaps identified, we have continued the development of the numerical model of LHD, which will be used in future CFD studies addressing the abovementioned gaps.

1.3. DTS system in tunnel fire detection

Linear Heat Detection (LHD) is based on distributed temperature sensing (DTS) is one of the most commonly applied technologies for fire detection. Many studies summarise the principles and application of DTS (Amira et al.; Fan et al., 2014; Guo et al., 2024; Silva et al.; Li and Zhang, 2022). It uses the optical Raman scattering, which is based on the assumption that when light enters the sensor fiber, its frequency changes due to the interaction of pulsed light with molecular motion. The pulsed signal changes into high-frequency anti-Stokes light or lower-frequency state Stokes light by emitting or absorbing optical phonons into or out of the sensor fiber. Using the optical reflectometry method, it could be monitored heated zone of the sensor cable (Dakin et al., 1985). The ratio between measured anti-Stokes and Stokes lines is expressed by equation (1)

$$R = \left(\frac{\lambda_{ASt}}{\lambda_{St}}\right)^4 e^{-\frac{hc\nabla}{kT}} \tag{1}$$

In the equation (1), λ_{ASt} and λ_{St} (nm) are Anti-Stokes and Stokes wavelengths, respectively, h is the Planck's constant, c (m/s) is the speed of the light, ∇ (cm $^{-1}$) is the wave number separation between Raman and Rayleigh light for a given fiber optic, k is the Boltzmann constant, T is the absolute temperature (K) of zone exposure to hot gases. Saxena et al. (Kumar Saxena, et al., 2022) presented that temperature value is computed using the modified equation (1), given by equation (2), where subscript θ and T correspond to ratio R value for the calibration zone and experimentally obtained actual signal profile, respectively.

$$T = \left(\frac{\left(\frac{h_{C}\nabla}{k}\right)}{\frac{h_{C}\nabla}{k}\frac{1}{\theta} - \ln\left(\frac{R_{T}}{R_{\theta}}\right)}\right) \tag{2}$$

The distributed temperature sensing relies on the effective Raman-Optical Time-Domain-Reflectometry (OTDR) technique. This technique operates by sending an optical laser pulse through the fiber, causing it to scatter and reflect back to the transmitting end for detailed analysis. The temperature along the length of the fiber is precisely determined by examining the intensity of the Raman signals present in the backscattered light, which encompasses a broad range of wavelengths. Some of these wavelengths are sensitive to temperature changes, while others remain unaffected. An accurate and comprehensive temperature measurement can be achieved by carefully analysing the variations in signal intensity across these different wavelengths. By measuring the arrival time of the returning light pulse, the local position of the temperature can be determined.

A complete fire detection system consists of several interconnected elements. The sensing element is a cable containing an optical fiber exposed to a fire plume from a burning vehicle. As a result of heating the optical fiber by fire gases, its structure changes according to the mechanism described earlier, which is detected by the reflectometer. Then, the reflectometer process backscattered light measurement raw data, named further log ratio, into temperature value, including individual calibration parameters for each tunnel. The data is transmitted to a computer unit with the appropriate detection system software, where the temperature profiles from the measurements are displayed. The sequence of steps in fire detection is presented in Fig. 1. When the vehicle ignites and stops ①, the sensor cable mounted on the tunnel ceiling is exposed to hot gases in the fire plume ②. The glass molecules in the fiber-optic core are subject to high temperature and change their structure ③. This causes the light to scatter in the laser beam ④ emitted by the Optical Time Domain Reflectometer ⑤. The OTDR is connected to the stationary computer unit of the tunnel infrastructure (6), where the dispatcher can view the history and real-time temperature measurement ①. This data is processed, compared with set criteria, and used to trigger an alarm. At the same time, a real-time display of results allows information to be passed on to the tunnel operator.

DTS systems in actual tunnels may vary in the resolution of temperature points and the time interval of these measurements. Adjusting the system settings usually involves coupled optimisation of the precision of temperature measurement and the data recording interval. They mainly depend on sensor cable length, signal loss, splices, and connectors. In road tunnels, temperature profiles are typically recorded every 0.5-2 m at 30-60 s intervals. In the early stage of fire growth, the fire location is detected as a hot spot on the temperature profile of the entire tunnel. Collecting data from all measurement intervals during an actual vehicle fire makes it possible to visualise the fire development process as the flow of smoke and hot gases, including the influence of the activation of the smoke control system. Fig. 2 presents an example of temperature profile history fire, log ratio and signal loss measured during the 350 kW fire test carried by the Authors in the road tunnel in Świnoujście, Poland, described in detail in Section 5. As the results show, recorded signal loss is correlated with the distance from the laser beam emitter and does not change with the sensor cable's temperature increase. It is a feature of the general performance of fiber-optic signal transmitting than a factor determining fire detection.

2. Methodology

2.1. Approaches for approximation of the heat transfer coefficient and RTI value

The functionality of the DTS system was incorporated in numerical modelling through a proposed approach based on heat transfer from the gas phase to the thin solid cylinder with the neglected effect of the Raman scattering phenomenon inside the fiber. It was assumed that the temperature of the glass fiber optic equals the temperature measured by the DTS system. The sensor's temperature rise was calculated according

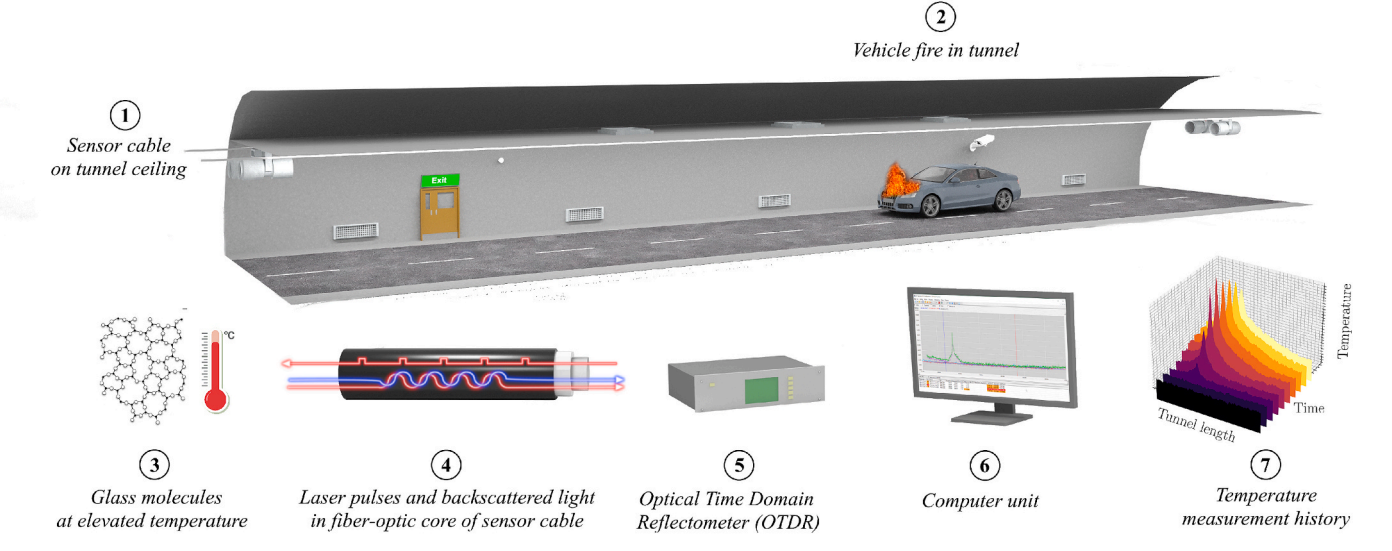


Fig. 1. The mechanism and sequence of linear heat detection based on DTS in tunnel fire.

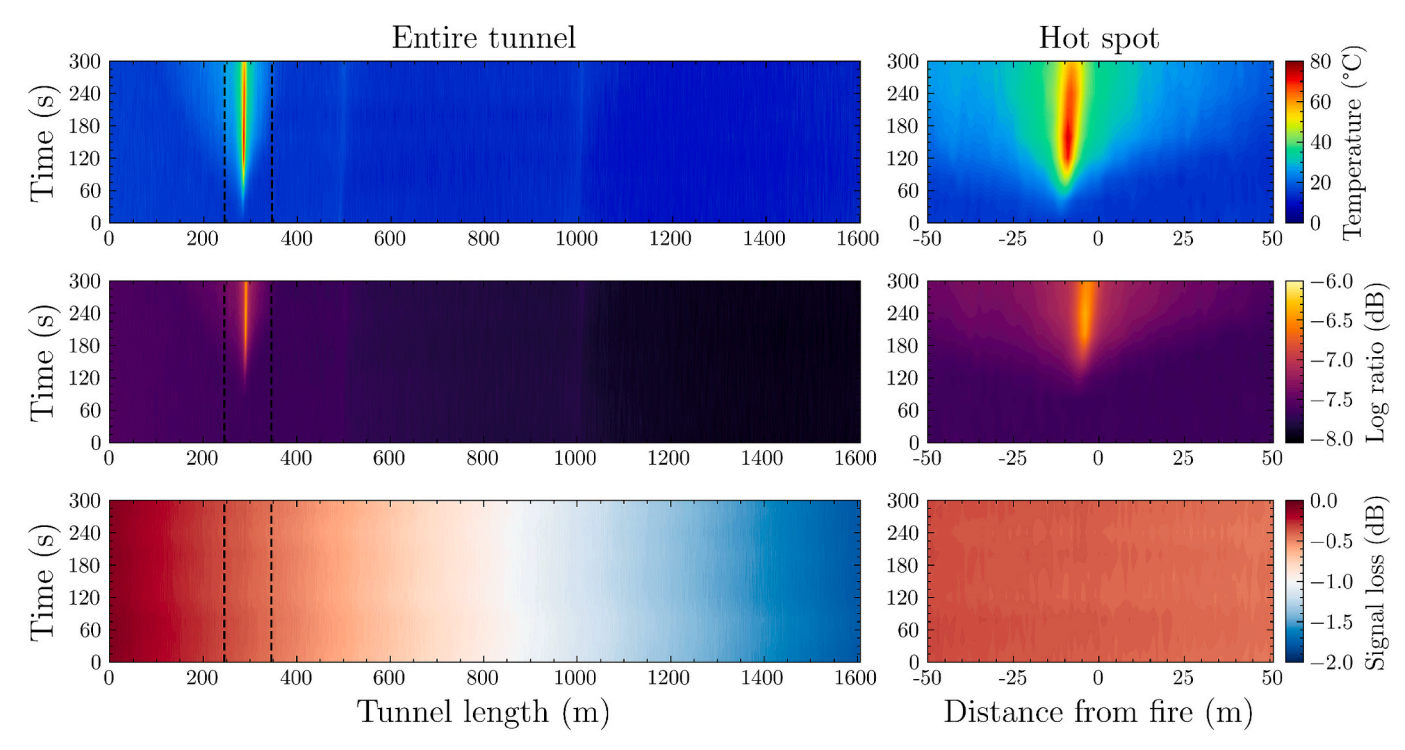


Fig. 2. Longitudinal temperature profile evolution and the raw signal measurements in the tunnel during the fire test. The X-axis presents the tunnel length, the Y-axis presents the time, and the colormap scale indicates measured temperature, log ratio and signal loss.

to the transient energy balance in the following equation (3).

$$\frac{D_{DTS}}{6}\rho_{DTS}C_{p,\ DTS}\frac{dT_{DTS}}{dt} = \epsilon \left(\frac{I}{4} - \sigma T_{DTS}^4\right) + h_c \left(T_{gas} - T_{DTS}\right) \tag{3}$$

In equation (9), D_{DTS} is the diameter of the cylinder (0.005 m), ρ_{DTS} is the density DTS sensor cable, $C_{p,DTS}$ is the specific heat of the DTS sensor cable, T_{DTS} is measured temperature by the DTS system, ϵ is radiation emissivity, I is incident radiation, σ is Stefan-Boltzmann constant, h_c is convective heat transfer coefficient, T_{gas} is the local temperature of the gas phase depends on fire plume flow. $D_{DTS}/6$ represents area of the sensor, and is derived with equation (4) (McGrattan, 2025).

$$A_{\text{spec}} = \frac{\frac{4}{3}\pi \left(\frac{1}{2}D_{DTS}\right)^{3}}{\pi \left(\frac{1}{2}D_{DTS}\right)^{2}} = \frac{D_{DTS}}{6}$$
 (4)

It is essential to consider forced convection into the optical fiber. Convective heat transfer coefficient for discrete body is calculated using equation (5).

$$h_c = Nu_D \left(\frac{k_g}{D}\right) \tag{5}$$

Thermal conductivity values of air k_g in the function of temperature was interpolated from the study (Stephan and Laesecke, 1985). The Nusselt

number Nu_D was calculated using correlation proposed by Churchill and Bernstein (Churchill and Bernstein, 1977); (Bergman et al., 2019) for circular cylinder body in crossflow, expressed by the following equation (6).

$$Nu_D = 0.3 + \frac{0.62 Re_D^{1/2} Pr^{1/3}}{\left[1 + \left(0.4/Pr\right)^{2/3}\right]^{1/4}} \left[1 + \left(\frac{Re_D}{282000}\right)^{5/8}\right]^{4/5}$$
 (6)

where Pr and Re_D are Prandtl number, and particle Reynolds number, are given by equations (7–8).

$$Pr = \frac{\nu}{\alpha} \tag{7}$$

$$Re_D \equiv \frac{\rho v D}{\mu} = \frac{Dv}{v} \tag{8}$$

Convective heat transfer plays a significant role when heating thin cylindrical- or particle-shaped bodies. Value of h_c increases rapidly as the airflow speed increases, which causes a faster temperature increase in the heated thermoelement. Fig. 3 shows a graph illustrating changes in h_c as a function of local air velocity and temperature for a DTS optical fiber with a diameter of 0.005 m exposed on airflow.

A pragmatic approach to heat detector activation in fire analyses is a simplified heat transfer concept proposed by Heskestad, named the response time index (RTI). The thermal properties of a device (sprinkler bulb, sensor) are summarised in a single value of the RTI, and its value is determined experimentally. This model is characterised by the assumption of the neglected effect of radiation in an early stage of fires and heat loss due to conduction to other parts of the detector. Temperature rise depends only on convective heat transfer. The RTI approach may beused to map the response time in fires in 3D space, as proposed in (Węgrzyński et al., 2020) The RTI, quantified in unit $(m/s)^{1/2}$, heat transfer form of DTS cable is expressed by the equation (7).

$$\frac{dT_{DTS}}{dt} = \frac{u^{1/2} \left(T_{gas} - T_{DTS}\right)}{RTI} \tag{7}$$

The manufacturers do not provide the RTI value for DTS sensor. From the laboratory experiments in the wind tunnel and through the best-fit approach to the numerical data, we have approximated the value of 90, which can potentially be used in the simplified modelling of the DTS performance.

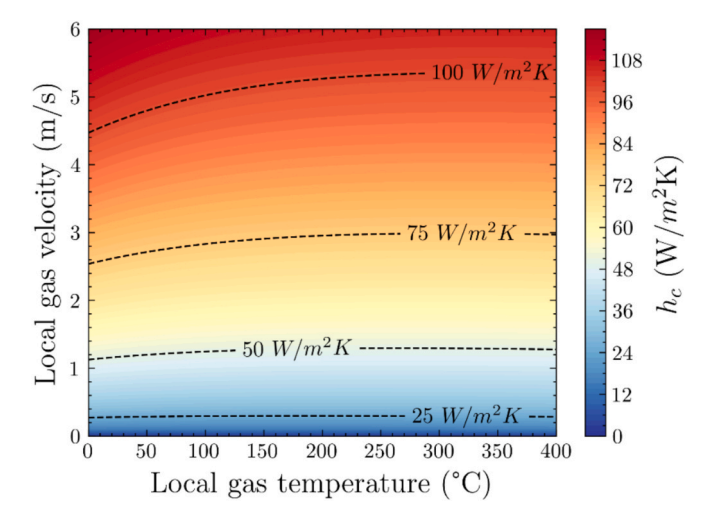


Fig. 3. Convective heat transfer coefficient in function of airflow velocity and temperature for 5 mm diameter cable.

2.2. Wind tunnel experiments

To efficiently model the performance of DTS sensor element, its thermal properties (thermal inertia) must be known. In addition to the heat transfer aspect, there is an additional aspect of the physics of Raman scattering in the glass molecules structure of the cable sensing. The product manufacturers do not share the cable properties. In order to determine the thermal properties of the cable influencing the temperature record delay, we have performed a series of calibration tests using a standardised EN 54–5 (EN 54-5; 2018) wind tunnel apparatus for fire heat detectors (see Fig. 4). The apparatus was equipped with a control unit for the fan and heater, which provided constant and homogenous velocity and temperature conditions. This allowed us to expose the cable to a range of well-defined velocity and temperature conditions and measure the cable response in a function of time. The same sensing cable was used in the wind tunnel tests as in the validation tests described further.

In the square duct of the wind tunnel with a cross-section of 0.4 m x 0.4 m, there was a 2 m long coiled section of optical fiber (4 measurement points) connected to the DTS configurator. The optical fiber was exposed to airflow at the following velocities: 0.5 m/s, 2.0 m/s, and 4.0 m/s at a constant temperature of $60\pm0.2\,^{\circ}\text{C}$. The selected velocities are representative of almost windless, low, and moderate airflow velocities in the tunnels, respectively, and highlight the importance of convective heat transfer discussed later. The temperature rise measured by DTS was recorded at 10-second intervals. The experiment was initiated when the sensor was placed in the tunnel channel. Temperature and airflow were maintained and measured, and the DTS sensor response was recorded.

2.3. Full-scale model validation experiments

Full-scale fire tests for evaluation of DTS fire detection performance and CFD simulations for validation of the proposed numerical model of the DTS were conducted in the road tunnel in Świnoujście in Poland. This tunnel is a single-tube bi-directional road tunnel that provides a connection between two Polish islands Uznam and Wolin. The tunnel is 1.780 km long, built using the tunnel boring machine (TBM) method for 1.484 km under the Świna river strait, and cut and cover method in parts near portals. The total width of the road is 10.5 m, including two road lanes and evacuation pathways. The DTS sensor is located above each road lane. In the Świnoujście Tunnel, a semi-transverse ventilation system was applied, and an extraction shaft with fire dampers was installed in the upper part of the TBM cross-section above the carriageway. However, the experiments were carried out without any smoke extraction. Internal airflow was entirely driven by natural draught. As shown in Fig. 5, the extraction shaft has an irregular shape, and the longest dimension of height in road space, from road to shaft slab, is 5.9 m.

To investigate the operation of the fire detection system in the road tunnel, we performed experiments with a pool fire located on the axis of the carriageway. The fire source was $20~\rm dm^3$ of *iso*-propanol, placed in 4 steel trays with dimensions $0.5~\rm m$ x $0.5~\rm m$ located side by side, with a total surface area of $1~\rm m^2$, directly below the sensor cable mounted on the ceiling. The actual heat release rate was not measured during the tests but was estimated using the fuel-burning regression rate in laboratory conditions as a value of approx. $350~\rm kW$. This value is representative of the initial phase of a vehicle fire in a tunnel, as typical peak HRR values for fully-developed passenger vehicle fires are $5,000-10,000~\rm kW$, reaching up to $30~\rm min$ (NFPA 502, 2023; Hodges et al., 2024; PIARC, 2017). The experimental setup and tunnel equipment used for measurement are presented in Fig. 6. Two scenarios were carried out, one in quiescent wind conditions (initial flow velocity of $0.5~\rm m/s$) and the second with a longitudinal flow of approx. $1~\rm m/s$.

The DTS system manufactured by Honeywell was used for measurements and data acquisition. The DTS system is integrated with all safety systems in the tunnel facility using a SCADA integration system.

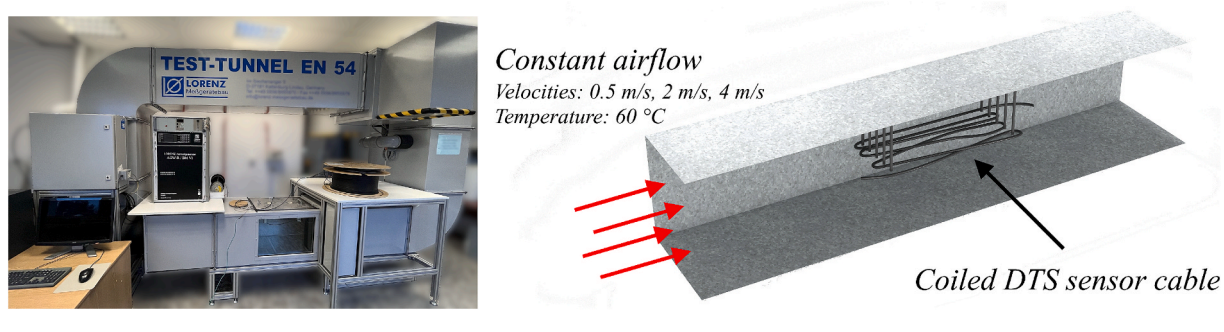


Fig. 4. EN 54-5 wind tunnel apparatus and test configurations.

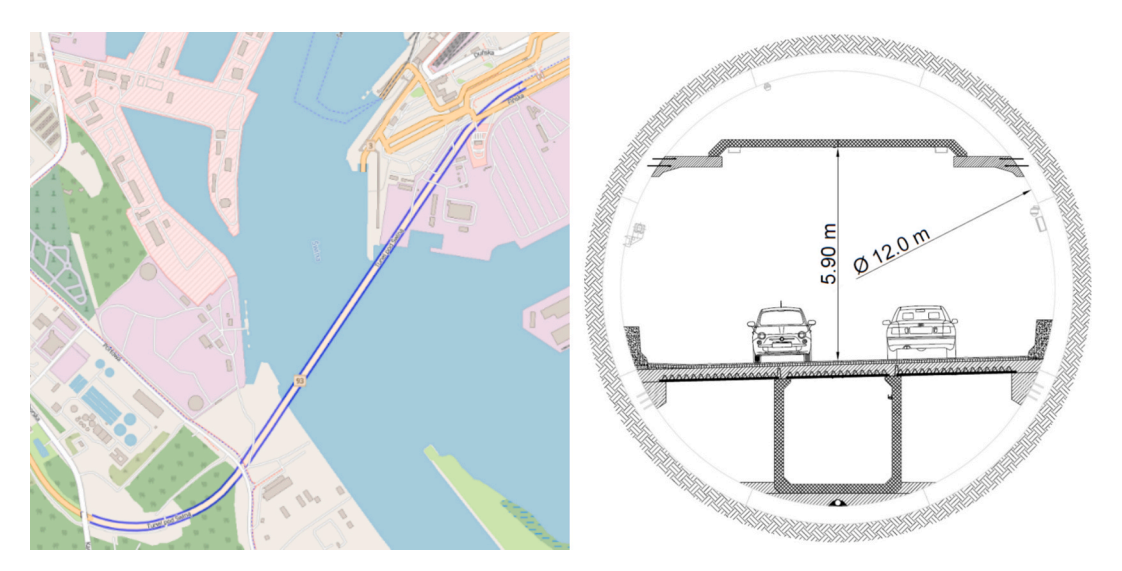


Fig. 5. Map of the Świnoujście tunnel and typical cross-section of the TBM sector.

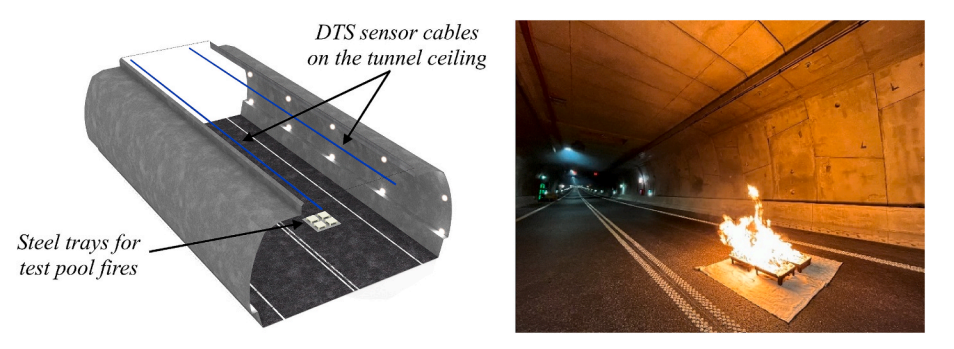


Fig. 6. Experimental setup and view of the typical fire test scene.

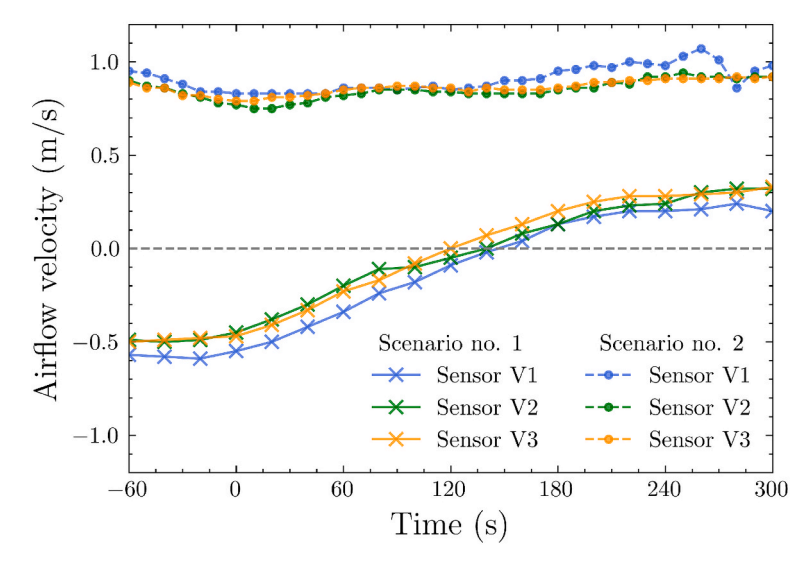
The DTS configurator setup can be changed to suit different alarm criteria and can be connected to a fire alarm control panel via relay inputs and outputs. The current airflow velocity was measured using three ultrasonic tunnel sensors: TunnelTech series TT801 manufactured by Codel, placed successively on road sections $0+951\ \mathrm{km},\,1+540\ \mathrm{km},$ and $2+130\ \mathrm{km}$ at 3.8—4.3 m heights. The sensors enable linear measurement of average air velocity in the tunnel.

The airflow conditions during the fire tests resulted from the natural draught caused by the wind. For this reason, obtaining absolute windless conditions in sufficient time to perform experiments is not feasible. Two fire tests were carried out, the first for calm conditions, where the initial air flow velocity was 0.35~m/s, and during the test, the airflow changed direction and reached a stable velocity of 0.25~m/s. During the second fire test, the velocity was stable from the beginning in the 0.8-1~m/s

range. A graph of the velocities recorded by three ultrasonic sensors is shown in Fig. 7. Negative values reflect the flow direction from east to west, while positive values reflect the direction from west to east.

2.4. Numerical modelling

CFD modelling is a widespread engineering tool that enables the prediction of the distribution of flow parameters, i.e. velocity, pressure, species mass concentration, and temperature, which is important for forecasting fire development and smoke spread in actual facilities. This is particularly valuable for tunnels, given the severity of typical vehicle fires, hazards for humans, and potential structural damage. In this study, ANSYS Fluent 19R1 CFD code was used. It is a commercial software based on the finite volume method (FVM) for general use in simulating



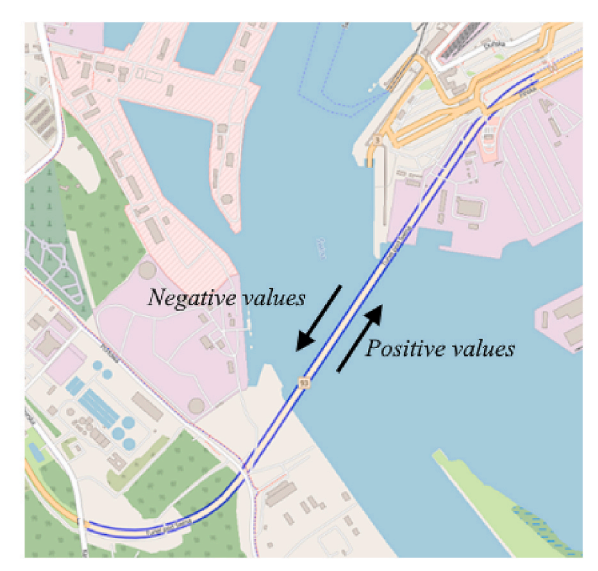


Fig. 7. Airflow velocity measurement during fire tests in road tunnel. Signs indicates directions for positive and negative values.

fluid flow with chemical reactions and heat transfer, and was previously used to simulate tunnel flows (Król et al., May 2024; Król et al., Sep. 2019) and fires (Beyer et al., Mar. 2024; Król et al., Nov. 2017). CFD modelling involves numerical solving governing partial differential equations (PDE) of fluid motion in 3-dimensional space. One of the principles is the continuity conservation equation, which defines that the fluid is treated as a continuous medium expressed by equation (8).

$$\frac{\partial \rho}{\partial t} + \nabla(\rho \, \overrightarrow{u}) = \mathbf{S}_{\mathbf{m}} \tag{8}$$

where S_m is the mass added to the fluid volume, such as combustible gas, into the burner area's surface. Chemical species transport in fluid motion is calculated using equation (9).

$$\frac{\partial \rho}{\partial t}(\rho \mathbf{Y}_i) + \nabla(\rho \overrightarrow{u} \mathbf{Y}_i) = -\nabla \overrightarrow{J}_j + R_i \tag{9}$$

where \overrightarrow{J}_i is mass diffusion flux of species i and differently calculated for laminar and turbulent flows, R_i is the net rate of production of species i by chemical reaction calculated using the Eddy-Dissipation Model (EDM) proposed by Magnussen and Hjertager (Magnussen and Hjertager, 1977). Conservation of momentum is the implementation of the Navier-Stokes equation expressed by equation (10):

$$\frac{\partial}{\partial t}(\rho \overrightarrow{u}) + \nabla(\rho \overrightarrow{u} \overrightarrow{u}) = -\nabla p + \nabla \bullet \overline{\overline{\tau}} + \rho \overrightarrow{g} + \overrightarrow{F}$$
(10)

In equation (5) p is static pressure, $\overline{\tau}$ is the stress tensor, $\rho \overrightarrow{g}$ are the gravitational body, \overrightarrow{F} represents external body forces. The energy conservation following equation (11).

$$\frac{\partial}{\partial t} \left(\rho \left(\mathbf{e} + \frac{\mathbf{u}^2}{2} \right) \right) + \nabla \left(\rho \mathbf{v} \left(\mathbf{h} + \frac{\mathbf{u}^2}{2} \right) \right) \\
= \nabla \left(\mathbf{k}_{\text{eff}} \nabla \mathbf{T} - \sum_{j} h_{j} \overrightarrow{J}_{j} + \overline{\tau} \overrightarrow{v} \right) + S_{h} \tag{11}$$

The energy source due to chemical reaction is defined as:

$$S_h = -\sum_j \frac{h_j^0}{M_j} R_j \tag{12}$$

In the equation, h_j^0 is the enthalpy of the formation of species j, M_j is the molecular mass of species j, R_j is the volumetric rate of creation of species j.

The simulations were performed in a transient mode with a fixed time step. The realizable $k\text{-}\epsilon$ model was used for turbulence modelling, classified as an Unsteady Reynolds-Averaged Navies Stokes (URANS) model. The fire phenomenon was simulated as a reacting fluid flow controlled by mixing using the Eddy-Dissipation Model (EDM) for turbulence-chemistry interaction and the Moss-Brookes model for soot (smoke) production. A list of general models and initial conditions is presented in Table 1.

Fire tests in the Świnoujscie tunnel were simulated using CFD to assess the feasibility of modelling the functionality of DTS fiber optics in tunnel fire detection. For this purpose, a full-scale geometrical model of the tunnel was prepared. Spatial discretisation was performed to a finite number of polyhedral control volumes. In the section of the tunnel where greater accuracy was required related to the flow of the fire plume, temperature and species concentration gradients, polyhedral elements with a size of $0.5-0.25~\mathrm{m}$ were used. In total, a numerical model of the tunnel Świnoujście consisted of cells. An additional five inflation layers with a growth rate equal to 1.1 were applied to boundary layers to improve flow conditions in DTS linear detector location regions.

Boundary conditions were implemented as appropriate for the case. Both tunnel portals constituted a *pressure-outlet* with free air inflow and outflow for the scenario in quiescent conditions. However, for the forced airflow scenario with constant velocity, the initial airflow value was 0.9 m/s, and one outlet from the tunnel was a *velocity inlet* to ensure a continuous flow at the set velocity. Numerical model of the tunnel

Table 1Numerical simulations setup.

Feature	Value		
Solver	Pressure-based, double-precision		
Turbulent flow and sub- models	Unsteady RANS, Reliazble k - ε		
Time step	Fixed, 0.5 s		
Radiation heat transfer	Discrete ordinates, WSGGM model		
Convective heat transfer	Tunnel walls: forced convection, $h_c = 35W/m^2K$ DTS fiber optic: cylinder body in cross flow eq. (10)		
Conductive heat transfer	Based on the Fourier law		
Combustion model	Species transport with EDM, 1-step chemical reaction		
Computational scheme	Coupled		
Gradient discretization	Green-Gauss Node Based		
Pressure discretization	Body Force Weighted		
Under-relaxation factors	ANSYS Fluent default		

domain is presented in Fig. 8.

Mesh sensitivity was performed for the study, investigating three sizes of meshes, as defined in Table 2. Fig. 9 illustrates the rise in the temperature for a test simulation with three meshes. A sensitivity analysis of the computational mesh was performed following the scheme. Longitudinal temperature profiles measured by DTS and the distance of the alarm triggering point from the fire location were selected as comparative parameters. It was noticed that medium and fine meshes represented the sensor's shape and time response well, while for coarse mesh, the distance at which the sensor was heated was greater. Therefore, it was chosen to apply the medium mesh for the study with the entire tunnel.

Obtain temperature profiles are presented in Fig. 9. The course mesh gave inaccurate results of time detection and location in both scenarios. Slight differences in temperature profiles were observed between medium and fine meshes. To optimize the computational cost, the mesh medium was chosen as an appropriate calibrated numerical model and compared results with experimental data.

3. Results and discussion

3.1. DTS model development

Tests carried out in the EN 54–5 (EN 54-5; 2018) wind tunnel using DTS fiber optic in laboratory conditions enabled a precise record of changes in optical signal ratio and temperature over time. A 2-meter section of optical fiber was in the wind tunnel space, divided into four measurement points every 0.5 m. The heated section shows a clear separation of the optical signal in the path of the laser beam through the optical fiber. The sensor cable was cooled after each test, and as the airflow rate increased, the difference between the loss before and after the hot air flow decreased. The recorded temperature rises at different rates at points exposed to a hot airstream. Fig. 10 shows each test's longitudinal DTS fiber optic profile of temperature changes and log ratio.

The sensing cable consists of several components: the outer jacket, aramid yarn, cable filling compounds and the optical fiber core. Based on tests in the wind tunnel, the estimated substitute values for the density and specific heat of the entire material were 5,800 $\,{\rm kg/m^3}$ and 950 kJ/kg·K. This resulted in satisfactory compliance with the method based on the principles of heat transfer, including convective heat exchange between the gas and the cylindrical sensor cable. However, the best compliance was obtained for RTI = 90 when using the response time index method. The average temperature measurement recorded by the DTS system in the wind tunnel and the results of the heat transferbased DTS model using equation (9) with substitute values and RTI method are shown in Fig. 11.

Based on temperature evolution could be distinguished by the heating phase up to $300\,\mathrm{s}$ of the test, and the constant temperature stage

Table 2
Meshes used in mesh-sensitivity study.

Mesh size	Coarse	Medium	Fine
No. of cells	510,693	897,871	1,745,145
No. of faces	2,539,937	4,410,887	8,766,651
No. of nodes	1,612,496	2,763,450	5,601,378
Fire source mesh size	0.05 m	0.05 m	0.05 m
Tunnel mesh size	0.5 m	0.35 m	0.25 m

to the end of the test. The proposed model based on ideal heat transfer reaches the nominal airflow temperature. However, there were some imperfections in the optical fiber measurement. The temperature measured by the cable sensor has not reached the airflow temperature. The average values of the sensor-measured temperature after the 300 s of the test were 54.86 $^{\circ}\text{C}$, 55.16 $^{\circ}\text{C}$, and 56.85 $^{\circ}\text{C}$ for the speed of 0.5 m/s, 2 m/s, and 4 m/s, respectively.

The obtain results shown some physical limitations of the measurement device for accurately measuring gas temperature. However, in the heating phase, a significant difference was observed in the rate of temperature increase depending on the air velocity. The temperature of a DTS sensor cable exposed to hot airflow increases faster as the airflow velocity increases. These observations highlight the importance of convective heat transfer. Fig. 12 shows the evolution of the temperature rate of rise in the heating phase. Regular fluctuations are observed in experiment temperature curves. It is probably caused by discrepancies in sensor cable or laser pulses for high-frequency time interval measurements.

3.2. DTS model validation

Such significant differences in DTS temperature measurements between scenarios 1 and 2 are directly due to the flow of the fire plume. The spatiotemporal flow properties in both cases were analyzed based on CFD simulations. In the first, hot gases are accumulated under the ceiling and a bidirectional flow occurs with a predominance towards the natural buoyancy resulting from the tunnel inclination. Stratification and a clear separation of the upper hot layer from the ambient cold air are observed. In the second scenario, there is a forced air flow in the tunnel, which affects the fire-driven flow. Fire gases mix with the ambient air, causing cooling of the fire plume. Fig. 13 shows the gas temperature of the spatial isosurfaces for 20, 30, 40, 50 and 60 $^{\circ}$ C at 120 s of each simulation. This time step represents the stabilized flow conditions for both scenarios. The trajectory of hot gases is crucial for the DTS measurement leading to triggering a fire alarm or absence of detection.

The experiment with a relatively low fire HRR in a real road tunnel has biases, mainly related to the difficult-to-measure airflow pattern in cross-section. The boundary condition of a stable air stream in the

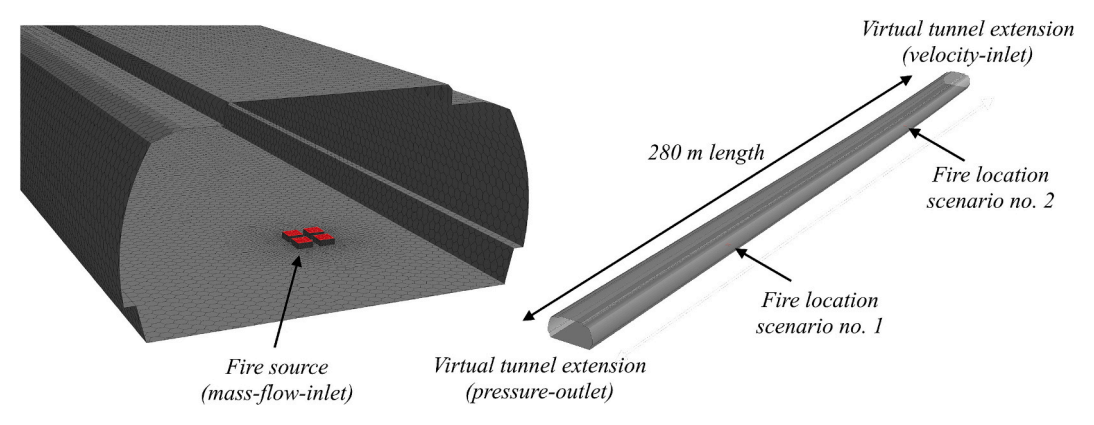


Fig. 8. Numerical model of Świnoujście tunnel fire test.

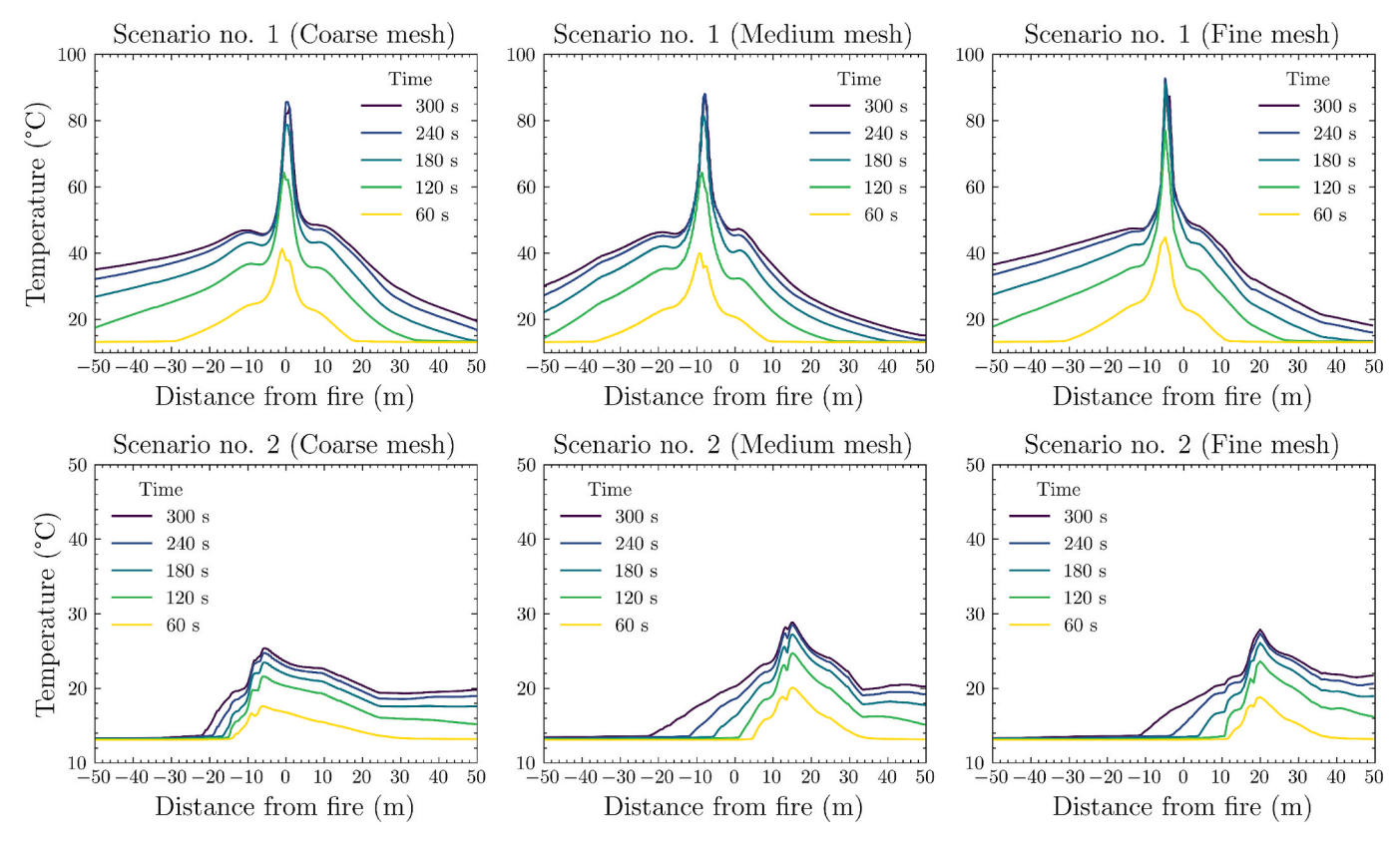
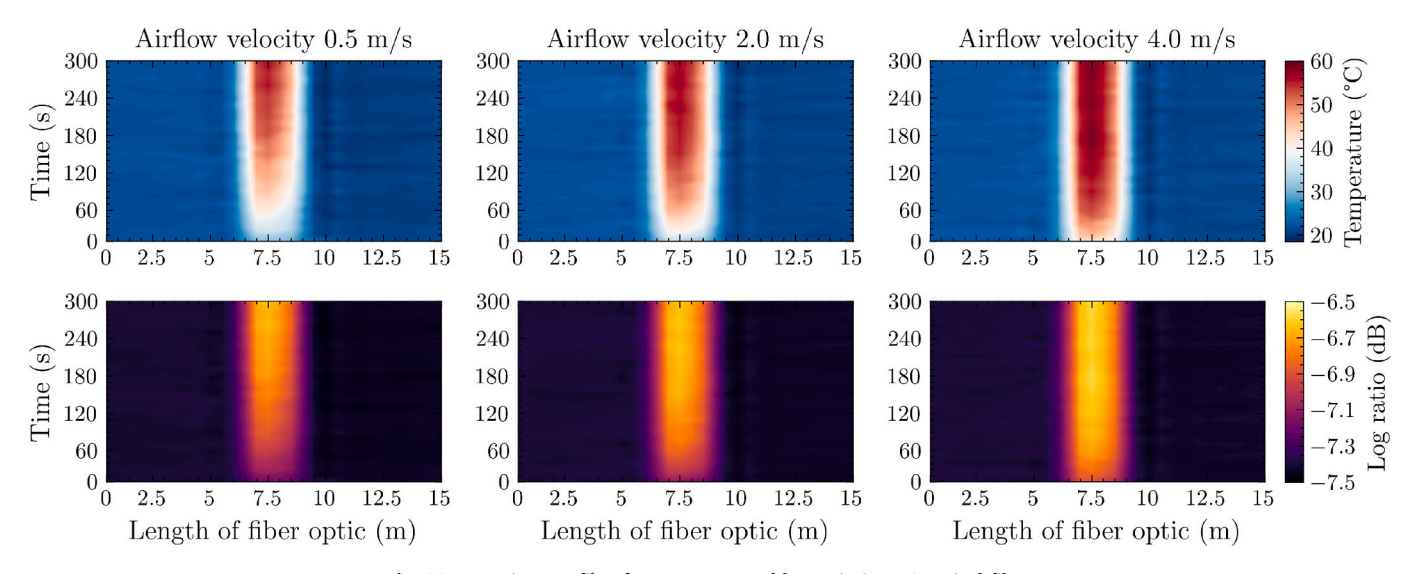


Fig. 9. Evolution in linear DTS temperature profile in mesh sensitivity.



 $\textbf{Fig. 10.} \ \ \textbf{Transient profile of temperature and log ratio in DTS optical fiber.}$

domain was implemented based on the measured air velocity averaged over time in 3 points of the Świnoujście tunnel during fire tests. Despite this, satisfactory precision in time and location was achieved in the predicted profile of temperature changes in the DTS cable. The history of the temperature profile from the experiment and numerical simulation is presented in Fig. 14. The DTS cable temperatures in the simulation exhibit a slightly higher temperature in the later phase of the fire (after 150 s), which is undoubtedly related to the phase of decreasing HRR in the experiment. A constant HRR equals 350 kW value was used in the simulation.

In scenario 1 at quiescent airflow conditions, the alarm was activated

by exceeding the absolute temperature criterion of 60 $^{\circ}$ C in experiments and simulations in 104.5 s and 107.6 s, respectively. The relative error of the numerical result is 2.97 %. The temperature profiles also indicate the stack effect of the flow of hot gases in the direction of inclination on the graph towards negative values of distance from the fire. The smooth characteristic of the temperature history profile is related to the URANS turbulence model.

Another characteristic feature of LHD is the temperature rate of rise in a certain time period. It could be set as another or equivalent criteria for triggering a fire alarm. The actual DTS system in the tunnel was calibrated for measuring temperature profiles in 40-second time in-

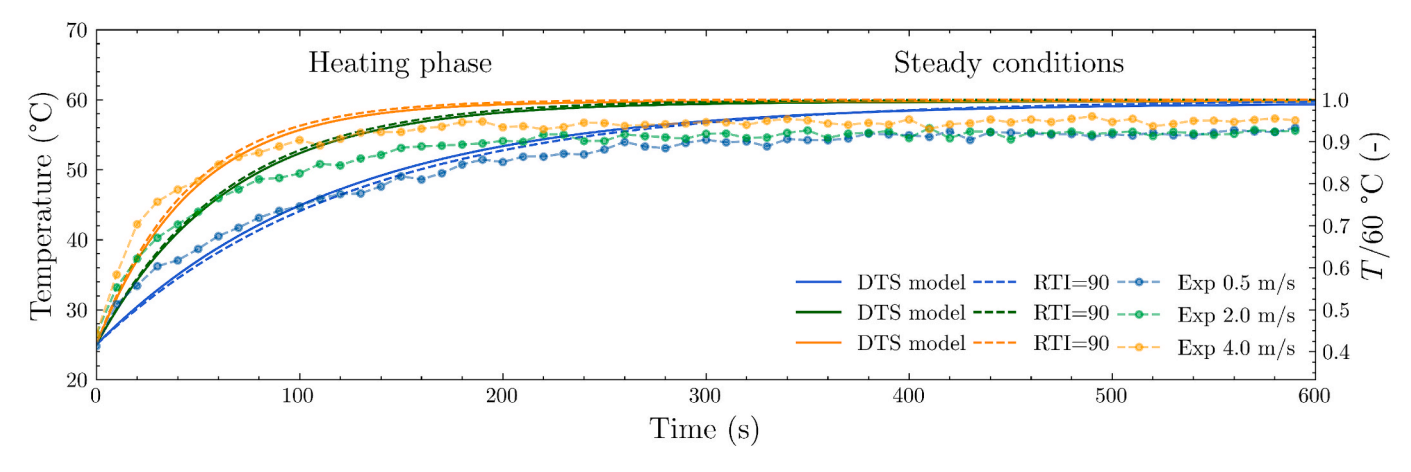


Fig. 11. Evolution of temperature measurement of DTS cable in wind tunnel test, DTS model and RTI model.

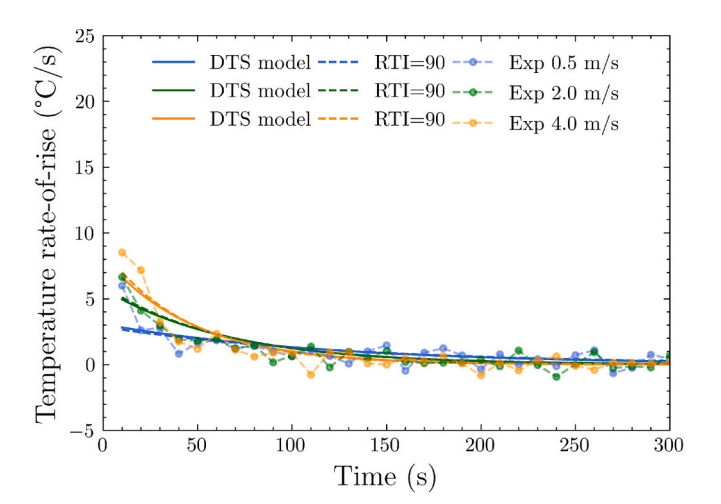


Fig. 12. Temperature rate-of-rise evolution in wind tunnel tests, DTS model and RTI model.

tervals. Fig. 15 shows a map of the evolution of ΔT over time until detection. The overall shape of temperature changes is convergent, but the rate of temperature increase is more smooth in the DTS model. Due to this, the highest ΔT values were not observed in the model as in the

experimental data.

In scenario 2, with a constant forced airflow of approximately 1 m/s, the DTS thermal response mapping accurately located the hot spot, but the model presented lower values than the experiment. A low HRR value and local air turbulence may significantly influence this. The difference between the highest values between the experiment and the simulation is 5.5 $^{\circ}$ C. Fig. 16 shows the temperature profile history for scenario 2. In this test, the alarm was not activated using either method. The hottest points of DTS were at a distance of 16–18 m from the fire origin in both CFD and the experiment.

Although the fire source conditions were the same, the forced air flow caused a significant reduction in the temperature measured by DTS in both methods. This highlights the significant role of considering airflow, especially in test fires in laboratory conditions and at the commission stage of actual tunnels.

4. Conclusions

This study examined the functionality of linear heat detection based on DTS technology for tunnel fires. Results reached from experiments and numerical simulations provide the following findings and conclusions:

 We have developed a distributed temperature sensor (DTS) model based on heat transfer principles through cylindrical objects.

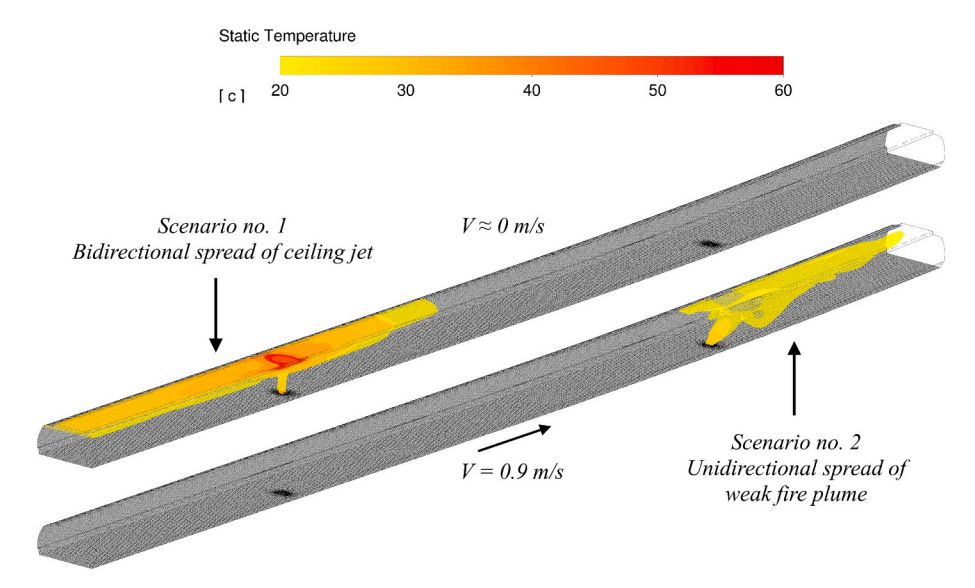


Fig. 13. Fire plume flow pattern in performed CFD simulations.

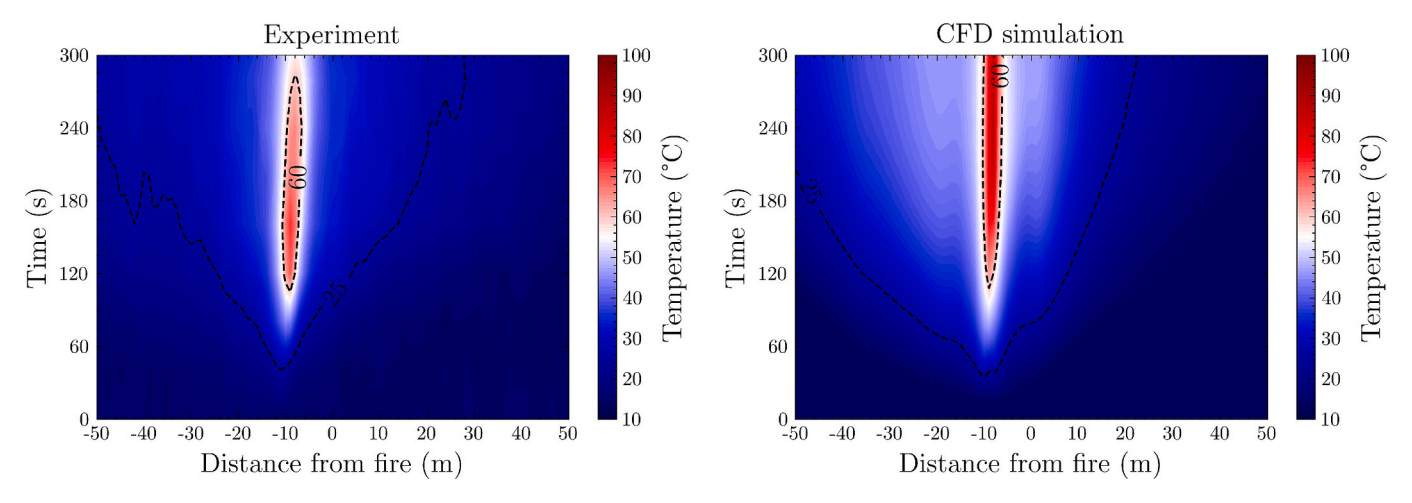


Fig. 14. Comparison of experimental and numerical DTS temperature profile in fire test at scenario no. 1 - quiescent airflow conditions.

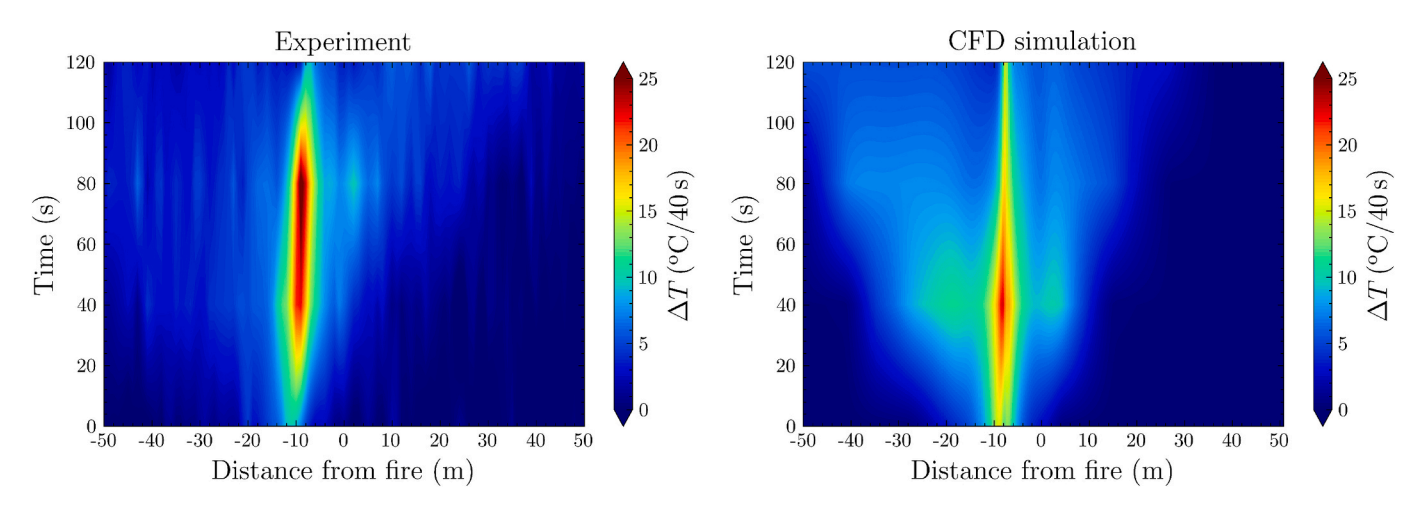
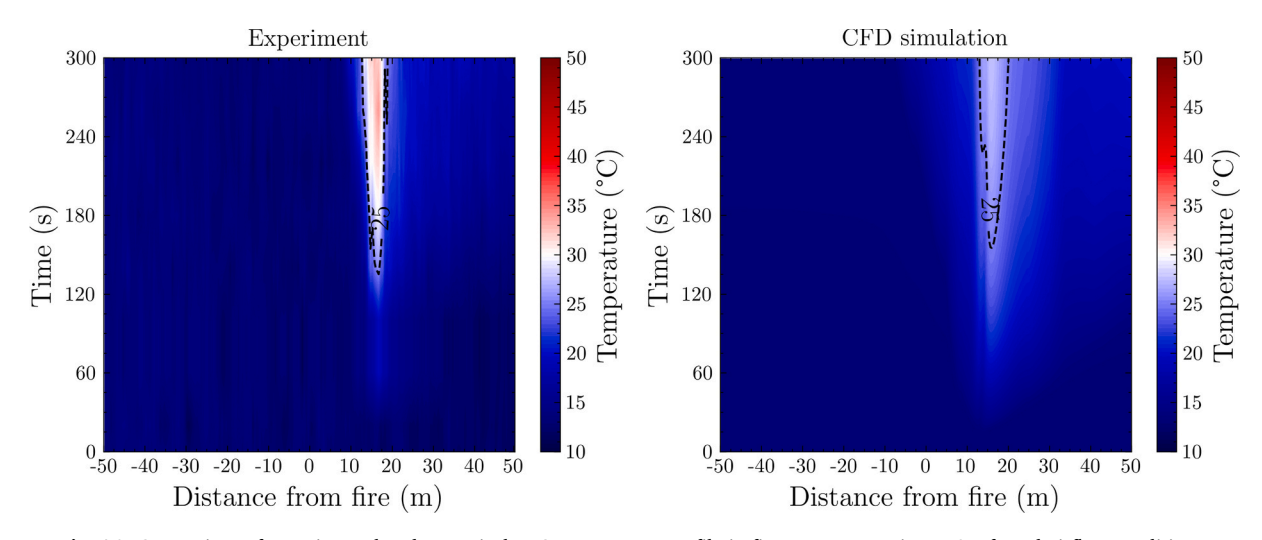


Fig. 15. Comparison of experimental and numerical temperature rise in the 40-second time interval.



 $\textbf{Fig. 16.} \ \ \textbf{Comparison of experimental and numerical DTS temperature profile in fire test at scenario no. 2-forced airflow conditions.}$

Substitute thermal properties of the cable found to match the experimental results and further used in the study were $5,800 \text{ kg/m}^3$ for the density and $950 \text{ kJ/kg} \cdot \text{K}$ for the specific. The convective heat transfer coefficient was defined with Churchill and Bernstein model (Churchill and Bernstein, 1977). This approach can be directly used

- in tunnel fire simulations using any CFD codes by implementation into the solver or at the postprocessing stage.
- 2) In the case of the simplified response-time index model proposed by Heskestad for heat sensors, we found a satisfactory match for the value of RTI = 90. Compared with the heat transfer model

- predictions, we concluded that this approach may also be successfully used for engineering calculations.
- 3) The LHD sensor has its thermal inertia, and numerical analyses of the fire detection time are performed based solely on gas temperature measurement. It may be significantly lower results than the actual alarm triggering time.
- 4) A fiber-optic DTS system is adequate for tunnel fire detection but could be insufficient in case of fires with low HRR. In our case, the fire with HRR of approx. 350 kW was undetected in an airflow velocity of 1 m/s. The airflow velocity in tunnels is commonly driven by the piston effect from vehicle movement or external wind into portals. Operational air velocity could reach and stabilise for 4–6 m/s. Fire plumes of weak fires could be destroyed by accelerated airflow and would not trigger alarms. For this reason, it seems prudent to support the LHD system by installing CCTV cameras to provide the tunnel operator with a view of traffic and current events. Furthermore, future studies on the response of LHD in real traffic and airflow conditions for various potential fire sources are justified.

Further research into linear heat detection in tunnel fires should investigate the impact of airflow conditions on alarm trigger time in more detail. The model proposed in this paper can be used to analyse fires with different HRR growth curves, fires of moving vehicles or utility tunnel fires, and other spaces equipped with distributed temperature sensors, providing a valuable tool in future parametric studies.

CRediT authorship contribution statement

Jakub Bielawski: Writing – original draft, Visualization, Validation, Software, Project administration, Investigation, Data curation, Conceptualization. Dia Luan: Writing – review & editing, Validation, Methodology, Conceptualization. Xiaoning Zhang: Writing – review & editing, Investigation, Data curation. Weikang Xie: Writing – review & editing, Visualization, Validation. Xinyan Huang: Writing – review & editing, Supervision, Methodology, Funding acquisition, Formal analysis. Wojciech Węgrzyński: Writing – review & editing, Supervision, Funding acquisition, Formal analysis, Conceptualization.

Declaration of competing interest

The authors declare that they have no known competing financial interests or personal relationships that could have appeared to influence the work reported in this paper.

Acknowledgments

This work was supported by the Ministry of Science and Higher Education of Poland Foundation, through the Building Research Institute statutory funding grant NZP-145/2024 and the first author contribution of the Research Student Attachment Programme of the Hong Kong Polytechnic University. The authors would like to thank the Honeywell Poland team for their valuable support. XH thanks the support from Sichuan Jiutong Smart Road Co. Ltd. (Goveste).

Data availability

Data will be made available on request.

References

- Amira, Z., Bouyahi, M., Ezzedine, T., Jan. 2015. Measurement of Temperature through Raman Scattering. Procedia Comput. Sci. 73, 350–357. https://doi.org/10.1016/J. PROCS.2015.12.003.
- ASTRA, 2007, ASTRA13 004, "Branddetektion in Strassentunneln," Bundesamt für Strassen (ASTRA).

- Bari, S., Naser, J., 2010. Simulation of airflow and pollution levels caused by severe traffic jam in a road tunnel. Tunn. Undergr. Space Technol. 25 (1), 70–77. https:// doi.org/10.1016/J.TUST.2009.09.004.
- Bergman, T.L., Lavine, A., Incropera, F.P., 2019. Fundamentals of heat and mass transfer, 8th ed. Wilev.
- Beyer, M., Stacey, C., Brenn, G., Mar. 2024. A mixed Convection Model for estimating the critical Velocity to prevent Smoke Backlayering in Tunnels. Fire Technol. 61 (2), 295–342. https://doi.org/10.1007/S10694-024-01607-8/FIGURES/19.
- Chen, T., et al., 2020. Study of flow characteristics in tunnels induced by canyon wind.

 J. Wind Eng. Ind. Aerodyn. 202, 104236. https://doi.org/10.1016/J.

 IWFIA 2020.104236
- Churchill, S.W., Bernstein, M., 1977. A Correlating Equation for Forced Convection from gases and Liquids to a Circular Cylinder in Crossflow. Journal of Heat and Mass Transfer 99, 300–306.
- Ciming Z., Liuyong C., Desheng J., Jun H., Shaoyun Z., 2007, Research and application of highway tunnel fire alarm system based on fiber Bragg grating sensor technology, Proceedings Volume 6595, Fundamental Problems of Optoelectronics and Microelectronics III; 659533 (2007) https://doi.org/10.1117/12.725901.
- Dakin, J.P., Pratt, D.J., Bibby, G.W., Ross, J.N., 1985. Distributed optical fibre Raman temperature sensor using a semiconductor light source and detector. Electron. Lett 21 (13), 569–570.
- EN 54-22:2015+A1:2020, "Fire detection and fire alarm systems Part 22: Resettable line-type heat detectors," 2020.
- EN 54-5:2017+A1:2018, "Fire detection and fire alarm systems Part 5: Heat detectors -Point heat detectors," 2018.
- Fan, D., Ding, H., Wang, D.Y., Jiang, D., 2014. Field test of optical and electrical fire detectors in simulated fire scenes in a cable tunnel. Photonic Sensors 4 (2), 156–161. https://doi.org/10.1007/s13320-014-0174-3.
- Guo, Z., Li, J., Hu, C., Li, Y., Su, Z., Xu, D., 2024. Comparative Analysis on Performance of Different Fire Detectors in Utility Cable Tunnel. Advances in Transdisciplinary Engineering 46, 584–590. https://doi.org/10.3233/ATDE231153.
- He, L., et al., 2021. Ceiling jet velocity during the whole process of fire development in a tunnel. J. Wind Eng. Ind. Aerodyn. 212, 104588. https://doi.org/10.1016/J. JWEIA.2021.104588.
- Hodges, J.L., Salvi, U., Kapahi, A., 2024. Design fire scenarios for hazard assessment of modern battery electric and internal combustion engine passenger vehicles. Fire Saf. J. 146, 104145. https://doi.org/10.1016/J.FIRESAF.2024.104145.
- Huijben J.W., 2002, Tests on fire detection system and sprinkler in a tunnel, ITC Conference Basel 2-4 December 2002.
- Ingason, H., et al., 2015. Development of a test method for fire detection in road tunnels.
- Ingason, H., Lönnermark, A., Li, Y.Z., 2012. Model of ventilation flows during large tunnel fires. Tunn. Undergr. Space Technol. 30, 64–73. https://doi.org/10.1016/J. TUST.2012.02.007.
- H. Ingason, Y. Z. Li, and A. Lönnermark, "Tunnel fire dynamics," Tunnel Fire Dynamics, pp. 1–504, Jan. 2015, doi: 10.1007/978-1-4939-2199-7/COVER.
- Ishii, H., Kawamura, K., Ono, T., Megumi, H., Kikkawa, A., 1997. A fire detection system using optical fibres for utility tunnels. Fire Saf. J. 29 (2–3), 87–98. https://doi.org/ 10.1016/S0379-7112(96)00065-3.
- Król, M., Król, A., Koper, P., Wrona, P., 2019. The influence of natural draught on the air flow in a tunnel with longitudinal ventilation. Tunn. Undergr. Space Technol. 85, 140–148. https://doi.org/10.1016/J.TUST.2018.12.008.
- Król, A., Król, M., Węgrzyński, W., 2023. A study on airflows induced by vehicle movement in road tunnels by the analysis of bulk data from tunnel sensors. Tunn. Undergr. Space Technol. 132, 104888. https://doi.org/10.1016/J. TUST.2022.104888.
- Król, A., Szewczyński, K., Król, M., Koper, P., Bielawski, J., Węgrzyński, W., 2024. Full-scale experimental, numerical, and theoretical research on the spatio-temporal evolution of the flow structure in longitudinal and semi-transversal ventilated tunnels. Tunn. Undergr. Space Technol. 147, 105721. https://doi.org/10.1016/J. TUST.2024.105721.
- Król, A., Szewczyński, K., Król, M., Koper, P., Bielawski, J., Węgrzyński, W., May 2024. Full-scale experimental, numerical, and theoretical research on the spatio-temporal evolution of the flow structure in longitudinal and semi-transversal ventilated tunnels. Tunn. Undergr. Space Technol. 147. https://doi.org/10.1016/j. tust 2024 105721
- Król, M., Król, A., Koper, P., Wrona, P., Nov. 2017. Full scale measurements of the operation of fire ventilation in a road tunnel. Tunn. Undergr. Space Technol. 70, 204–213. https://doi.org/10.1016/J.TUST.2017.07.016.
- Król, A., Król, M., Koper, P., Wrona, P., Sep. 2019. Numerical modeling of air velocity distribution in a road tunnel with a longitudinal ventilation system. Tunn. Undergr. Space Technol. 91. https://doi.org/10.1016/j.tust.2019.103003.
- M. Kumar Saxena et al., "Studies on thermal profile measurement and fire detection in a power supply cable of a synchrotron radiation source by Raman optical fiber distributed temperature sensor system," Optical Fiber Technology, vol. 73, p. 103020, Oct. 2022, doi: 10.1016/J.YOFTE.2022.103020.
- Li, Y.Z., Du, X., 2020. Fire tests with a line type heat detection system in the Runehamar tunnel. In: Proceedings from the Ninth International Symposium on Tunnel Safety and Security, pp. 529–544.
- J. Li and M. Zhang, "Physics and applications of Raman distributed optical fiber sensing," Light: Science & Applications 2022 11:1, vol. 11, no. 1, pp. 1–29, May 2022, doi: 10.1038/s41377-022-00811-x.
- Liang, C., Nan, S., Shao, X., Li, X., 2021. Calculation method for air resistance coefficient of vehicles in tunnel with different traffic conditions. Journal of Building Engineering 44. https://doi.org/10.1016/J.JOBE.2021.102971.

- Li, Y.Z., Lei, B., Ingason, H., 2011. The maximum temperature of buoyancy-driven smoke flow beneath the ceiling in tunnel fires. Fire Saf. J. 46 (4), 204–210. https://doi.org/10.1016/J.FIRESAF.2011.02.002.
- Li, Y.Z., Jiang, L., Ingason, H., 2020. Numerical modelling of a line type heat detection system in tunnel fires. In: Proceedings from the Ninth International Symposium on Tunnel Safety and Security, pp. 363–378.
- Liu, Z.G., Kashef, A.H., Lougheed, G.D., Crampton, G.P., 2011. Investigation on the Performance of Fire Detection Systems for Tunnel Applications-Part 2: Full-Scale Experiments under Longitudinal Airflow Conditions. Fire Technol. 47 (1), 191–220. https://doi.org/10.1007/s10694-010-0143-3.
- Liu, Z.G., Kashef, A.H., Lougheed, G.D., Crampton, G.P., 2011. Investigation on the Performance of Fire Detection Systems for Tunnel Applications-Part 1: Full-Scale Experiments at a Laboratory Tunnel. Fire Technol. 47 (1), 163–189. https://doi.org/ 10.1007/s10694-010-0142-4.
- Lönnermark, A., Hedekvist, P.O., Ingason, H., 2008. Gas temperature measurements using fibre Bragg grating during fire experiments in a tunnel. Fire Saf. J. 43 (2), 119–126. https://doi.org/10.1016/J.FIRESAF.2007.06.001.
- Luan, D., et al., 2021. Experimental investigation of smoke temperature and movement characteristics in tunnel fires with canyon cross wind. J. Wind Eng. Ind. Aerodyn. 210, 104531. https://doi.org/10.1016/J.JWEIA.2021.104531.
- Magnussen, B.F., Hjertager, B.H., 1977. On mathematical modeling of turbulent combustion with special emphasis on soot formation and combustion. Symposium (International) on Combustion 16 (1), 719–729. https://doi.org/10.1016/S0082-0784(77)80366-4.
- McGrattan, K., et al., 2025. Fire Dynamics Simulator User's Guide, Sixth Edition.
 National Institute of Standards and Technology.
- NCHRP, 2017. "NCHRP Research Report 836Guidelines for Emergency Ventilation Smoke Control in Roadway Tunnels". National Cooperative Highway Research Program.

- NFPA 502, 2023. Standard for Road Tunnels, Bridges, and Other Limited Access highways. National Fire Protection Association.
- NFPA 72, 2022. National Fire Alarm and Signaling Code®. National Fire Protection Association.
- PIARC, 2007, "Systems and equipment for fire and smoke control in road tunnels," World Road Association.
- PIARC, 2017. Design fire characteristics for road tunnels. PIARC.
- RABT, 2006. Richtlinie für die Ausstattung und den Betrieb von Straßentunneln, Forschungsgesellschaft für Straßen und Verkehrswesen," Forschungsgesellschaft für Straßen- und Verkehrswesen e.V.
- RVS, 2019, "RVS 09.02.22, 'Tunnel equipment'," Forschungsgesellschaft Straße Schiene Verkehr (FSV).
- Silva, L.C.B., Segatto, M.E.V., Castellani, C.E.S., Dec. 2022. Raman scattering-based distributed temperature sensors: a comprehensive literature review over the past 37 years and towards new avenues. Opt. Fiber Technol. 74, 103091. https://doi.org/ 10.1016/J.YOFTE.2022.103091.
- Stephan, K., Laesecke, A., 1985. The thermal Conductivity of Fluid Air. J. Phys. Chem. Ref. Data 14 (1), 227–234. https://doi.org/10.1063/1.555749.
- Wegrzyński, W., Lipecki, T., 2018. Wind and Fire coupled Modelling—Part I: Literature Review. Fire Technol. 54 (5), 1405–1442. https://doi.org/10.1007/S10694-018-0748-5/FIGURES/5.
- Wegrzyński, W., Krajewski, G., Tofiło, P., Jahn, W., Król, A., Król, M., 2020. 3D mapping of the sprinkler activation time. Energies 13 (6), 1450. https://doi.org/10.3390/EN13061450.
- Zeng, Y., Wong, H.Y., Wegrzyński, W., Huang, X., 2023. Revisiting Alpert's Correlations: Numerical Exploration of Early-Stage Building Fire and Detection. Fire Technol. 59 (5), 2925–2948. https://doi.org/10.1007/S10694-023-01461-0/FIGURES/16.
- Zhang, X., et al., 2021. Perspectives of big experimental database and artificial intelligence in tunnel fire research. Tunnell. Underground Space Technol. 108, 103691.